Development of highly permeable self-standing nanocomposite sulfonated poly ether ketone membrane using covalent organic frameworks

Myoung Jun Park[1†], Nawshad Akther[1†], Sherub Phuntsho[1], Gayathri Naidu[1], Amir Razmjou[1,2], Alicia Kyoungjin An[3], Ho Kyong Shon[1*]

[1] School of Civil and Environmental Engineering, University of Technology, Sydney, Post Box 129, Broadway, NSW 2007, Australia.

[2] School of Engineering, Edith Cowan University, Joondalup, Perth, WA 6027, Australia

[3] School of Energy and Environment, City University of Hong Kong, Tat Chee Avenue, Kowloon, Hong Kong, China

Abstract

This study developed a new symmetric and ultrathin membrane by incorporating Schiff base network-1 (SNW-1), which are covalent organic framework (COF) nanoparticles, as fillers in the sulfonated poly ether ketone (SPEK) matrix to improve forward osmosis (FO) performance. The amine-rich and porous SNW-1 nanoparticles enhanced the surface wettability of the SPEK membranes and offered additional passages for the water molecules' transport, which assisted in the elevation of membrane water flux. The modified membrane loaded with 20 wt% SNW-1 (COF-20) exhibited the best performance with a significantly higher water flux (28.5 L m^{-2} h^{-1}) and lower specific reverse solute flux (SRSF, 0.05 g L^{-1}) than that of the unmodified SPEK (COF-0) membrane (water flux of 12 L m^{-2} h^{-1} and SRSF of 0.16 g L^{-1}) when experimented

---

[†] Myoung Jun Park and Nawshad Akther equally contributed to this work.

[*] Corresponding Author: Email: Hokyong.Shon-1@uts.edu.au

with deionized water and 1 M Na_2SO_4 as feed and draw solutions, respectively. The impressive FO performances of nanocomposite SPEK membranes suggest that SNW-1 nanoparticles could be used as fillers for improving the SPEK membrane's performance in the FO application.

Keywords: Sulfonated poly ether ketone, forward osmosis, covalent organic framework, self-standing membrane, SNW-1

Highlights

- Free-standing and ultrathin nanocomposite SPEK FO membrane was synthesized.
- SNW-1 COF nanoparticles were used as fillers in SPEK membrane.
- SNW-1 pores provided more passages for water molecules' transport.
- Optimal COF-20 membrane revealed a water flux of 28.5 L m^{-2} h^{-1}.
- COF-20 membrane revealed a *SRSF* of 0.05 g L^{-1}.

1 Introduction

Water insufficiency is becoming a growing concern globally due to the rapid growth of population, urbanization and industrialization. Membrane separation is deemed to be the extremely favorable process among the currently existing water treatment and desalination technologies due to its high energy efficiency and ease of operation [1]. While process efficiency has been significantly improved using membrane technologies, efforts to develop new membranes and processes continue to further enhance energy efficiency and affordability. The forward osmosis (FO) is an evolving membrane separation process, which is powered by the difference in osmotic pressure existing between the high-concentrated draw solution (DS) and low-concentrated feed solution (FS) through a semi-permeable membrane [2, 3]. FO process can be directed to a wide array of applications, including wastewater treatment [4, 5], desalination [6, 7] and power generation [8, 9]. FO process has demonstrated remarkable characteristics, such as easy operation, low energy utilization, high rejection efficacy and low fouling tendency for several contaminants [10-12]. Nonetheless, the occurrence of internal concentration polarization (ICP) in asymmetric membranes significantly diminishes the available osmotic driving force, which substantially impedes performance and practical applications of the FO process [13]. Thus, membranes perform an important part in the FO process performance.

The thin-film composite (TFC) membrane encompassing of a porous substrate and an ultrathin selective dense polyamide (PA) layer (~200-300 nm) is mostly used in the FO process due to their excellent separation performance [14, 15]. However, the asymmetric nature of the TFC membranes influences the actual solute concentration at the active layer interface resulting in severe ICP [16, 17]. Several studies have reported strategies to mitigate ICP by enhancing the structural properties (membrane substrate’s thickness, tortuosity, pore-size distribution and porosity) [18, 19]. These techniques include, but are not confined to, modification of substrate preparation method [20-22]. Some researchers have also used highly porous and thin electrospun nanofibers as support layers for TFC membranes to mitigate ICP effects [23-25]. Although electrospun nanofiber substrates have successfully reduced the structural parameters of the TFC FO membranes, their large pore size causes delamination and defective formation of PA active layers.

In addition to substrate modification, dispersion of nanomaterial in the polymer matrix as fillers has also been explored to increase the permeability of the membranes [26]. Addition of nanomaterial influences membrane performance by altering membrane properties like morphology, porosity and hydrophilicity. Among the various nanomaterials reported in literature as fillers to prepare nanocomposite membranes are zeolite [27, 28], silica [7, 29], carbon nanotubes [30, 31], graphene oxide [32-35], titanium dioxide [36, 37] and covalent organic frameworks (COFs) [38-40].

Besides, self-standing FO membranes have also been investigated to reduce the structural parameter of membranes [41, 42]. Liu et al. [43] synthesized a 100 nm thick self-standing ultrathin reduced graphene oxide (rGO) membrane, which exhibited roughly five times greater water flux than the commercial cellulose triacetate FO membrane. Also, the ultrathin membrane nearly eliminated ICP. Yuan et al. [41], in contrast, fabricated a self-standing FO membrane from polysulfone through solvent evaporation method followed by doping the nanofilm with sulfonated polysulfone. The thinnest nanofilm with a 46 nm thickness demonstrated the highest water flux of 46 L m^{-2} h^{-1} and a specific reverse solute flux (SRSF) of 0.12 g L^{-1} with 1.25 M Na_2SO_4 as the DS and DI water as the FS. Li et al. [42] reported the synthesis of a symmetric and selective self-standing thin film membrane using a COOH-derived polyoxadiazole copolymer. The membrane showed excellent FO performance with an impressive water flux and a very high selectivity to Na_2SO_4 DS. Also, the ICP effect in the membrane was found to be negligible. Recently, our group reported the synthesis of an ultrathin, self-standing and symmetric FO membrane with a thickness of 600 nm using sulfonated poly ether ketone (SPEK) [14]. With DI water FS and 1 M NaCl DS, the membrane revealed a FO water flux and SRSF of 20.5 $L.m^{-2}.h^{-1}$ and 1.2 g L^{-1}, respectively.

In this study, we incorporated a melamine-based amine-rich covalent organic framework (COF), called Schiff base network-1 (SNW-1), as nanofillers in the self-standing SPEK membranes to improve the FO performance. COFs are organic crystalline two or three-dimensional porous structure with extended organic functional group structures made of light elements (H, C, B, O and N) that are connected by strong covalent bonds [38]. The large surface area, thermal stability and porosity of COFs make them extremely desirable as membrane fillers compared to most inorganic nanomaterials. Due to the favourable characteristics of COFs, they have found great interest in the applications like desalination, catalysis, adsorption, gas separation and photoelectricity [44-46]. Unlike metal-organic frameworks (MOFs), which are also three-dimensional porous coordination polymers, SNW-1 is highly stable in water, and thus has a great potential to be used as a nanofiller to fabricate composite membranes for liquid separations [45]. The SNW-1 COF nanoparticles were chosen as the suitable fillers for SPEK membrane modification in this study as they possess various desirable properties. For instance, SNW-1 has a porous structure with a pore size of 5.5 Å, which is larger than the size of a water molecule (3 Å) but smaller than that of salts like NaCl (5.64 Å) and Na_2SO_4 (7.6 Å), thus allowing high ion selectivity in FO process [44, 45]. The presence of amine groups in SNW-1 nanoparticles facilitates good dispersion and stability in the aqueous phase, improves membrane wettability. In addition, the small spherical size of SNW-1 nanoparticles (20–40 nm) is crucial for reducing membrane defects. The morphology, roughness, hydrophilicity and FO performance of the developed self-standing membrane were investigated by changing the loadings of SNW-1 nanoparticles and compared to the commercial TFC membrane. The novelty of this work is the development of a self-standing COF-incorporated SPEK FO membrane.

2 Materials and methods

2.1 Polymer, COF and membrane synthesis

Sulfonated poly ether ketone polymer with a sulfonic acid content of 40 mol% (SPEK-40) was synthesized using 3,3'-disulfonated-4,4'-difluorobenzophenone (DSDFBP), 4,4’-difluorobenzophenone (DFBP), tetramethyl bisphenol F (TMBPF), dimethyl sulfoxide (DMSO), potassium carbonate and toluene, which were supplied by Mitsui Chemicals, Inc (MCI). The details of SPEK-40 polymer synthesis methods are described in our previous work

[14]. SPEK-40 polymer blend was used in this study as it offered the optimally balanced polymer structure appropriate for the fabrication of self-standing membranes [14].

Terephthalaldehyde (99%), dimethyl sulfoxide (DMSO, 99.9%) and melamine purchased from Sigma-Aldrich, tetrahydrofuran (THF, 99%) and dichloromethane (DCM, 99.99%, VWR) and acetone (99.8%, Merck) were utilized for COF synthesis. A solvothermal method was used to produce the SNW-1 COF nanoparticles. Detailed COF synthesis and characterization methods are described and discussed in our previous work [40]. The synthesized SNW-1 nanoparticles in this study have a particle size of 20–40 nm and pore size of 5.5 Å as shown in our previous study using SEM images and Horvath-Kawazoe (HK) method, respectively.

The self-standing nanocomposite membranes were prepared from SPEK-40/COF dope solution using the film coating method. First, COF nanoparticles at various loadings (0 to 30 wt% with respect to the weight of SPEK) were dispersed in polymer solvent, methylene dichloride (MC), via ultrasonication for 1 hr. Next, 4 wt% SPEK-40 powder was dissolved in the COF/MC dispersion via continuous stirring overnight to attain the dope solution, which was then put aside to degas at 32°C for 6 h. Subsequently, the degassed dope solution was cast on a polyethylene terephthalate (PET) film supplied by MCI using an automatic film applicator and a casting knife with its gate height set to 80 µm at ambient conditions (humidity: 40 – 60%). The cast polymer film was then immediately put in an oven at 80ºC for 10 min to remove MC by evaporation. Finally, the COF-SPEK membrane was peeled off the PET film, placed in the middle of two nonwoven polyester fabrics and stored for testing and characterization. The overall procedure of the preparation of the COF-SPEK membranes is illustrated in Figure 1. Unlike the pristine SPEK membranes, which were transparent, the COF-SPEK membranes were opaque and white due to the incorporation of COF nanoparticles in the SPEK.

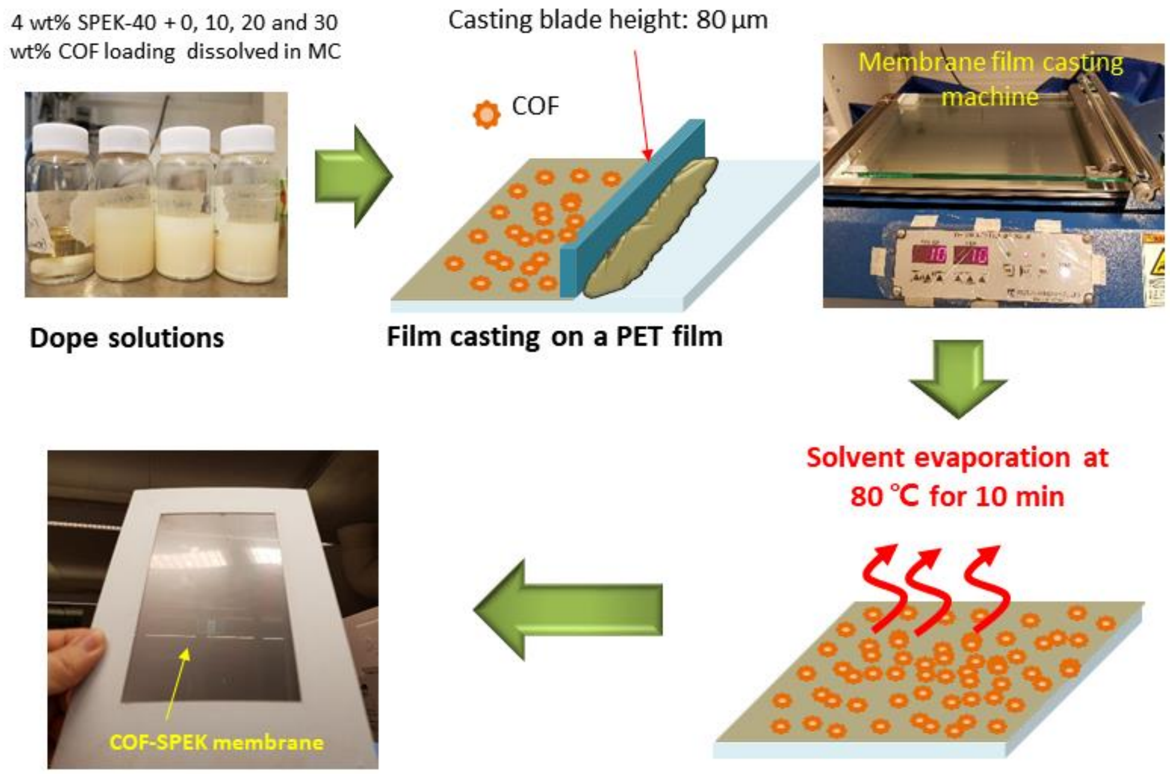

Figure 1. Schematic of COF-SPEK membrane fabrication.

2.2 Membrane characterization

Fourier transform infrared spectroscopy (FTIR, Shimadzu MIRacle 10) was used to identify the pristine and nanocomposite SPEK membranes' chemical compositions. The membrane cross-section and surface images were acquired at 5 kV with field emission scanning electron microscopy (FE-SEM, Zeiss Supra 55VP). A sputtering coater was used to coat the membrane samples with gold-palladium before SEM imaging. The membrane morphology and surface roughness were examined with atomic force microscopy (AFM, Dimension 3100, Bruker). The membranes wettability was established by determining the water contact angles with an optical tensiometer. For each membrane sample, the contact angles were randomly determined on at least six different locations on the membrane surfaces and the average was reported. The evaluation of mechanical properties of COF-SPEK membranes was performed using an

Advanced Materials Testing Machine (LS1, Lloyd instruments Ltd., UK) and the detailed protocols are demonstrated elsewhere [32].

2.3 Membrane performance evaluation

The fabricated FO membranes were tested using a laboratory-scale FO system as described in our earlier work [14]. The membrane sample was placed in an acrylic FO cell with flow channels measuring 2 cm long, 2 cm wide and 0.3 cm deep (effective membrane area of 4 cm^2). The FS and DS were co-currently circulated in batch mode at a specific crossflow rate of 300 $mL\cdot min^{-1}$ using two gear pumps (Cole Palmer). The FS and DS temperature was retained at 25°C with a computerized temperature control system attached to a water bath. The initial DS and FS volumes were fixed at 1 L each. Water flux was assessed using a digital balance connected to a PC that continuously recorded the change in DS weight over time. The reverse solute diffusion was calculated from the electrical conductivity measurements of the FS. Sodium sulfate (Na_2SO_4) was used as the DS, since it shows a low reverse solute flux due to the presence of divalent ion of SO_4^{2-}, and DI water as the FS during FO tests.

The water (J_W, L m^{-2} h^{-1}) and reverse solute (J_S, g m^{-2} h^{-1}) flux across the membrane was evaluated from Eq. 1 and Eq. 2, respectively.

$$J_W = \frac{\Delta\, V_{DS}}{A_m \times \Delta t} \tag{1}$$

$$J_S = \frac{\Delta C_{FS} \times V_{FS}}{A_m \times \Delta t} \tag{2}$$

where ΔV_{DS} (L) is the volume change of the DS, ΔC_{FS} (g L^{-1}) and V_{FS} (L) are the change in FS concentration and the FS volume when the experiments finish, respectively. Δt (h) and A_m (m^2) are the operation time and active membrane area.

Since higher solute concentration difference across the membrane generates both higher water and reverse solute flux, the ratio of J_S to J_W, is utilised to obtain the specific reverse solute flux (*SRSF*, g L^{-1}), which is a crucial membrane parameter in the FO process for determining the membrane selectivity (Eq. 3) [18, 35].

$$SRSF = \frac{J_S}{J_W} \tag{3}$$

Reverse osmosis (RO) tests for COF-SPEK membranes were conducted to determine the water permeability coefficient (*A*, L m^{-2} h^{-1} bar^{-1}), solute permeability coefficient (*B*, L m^{-2} h^{-1}) and Na_2SO_4 rejection (*R*, %). All samples were tested using a customized membrane cell with an active membrane area of 2 cm × 2 cm under the applied pressure of 10 bar at 25°C. For evaluating rejection performance, 2 g L^{-1} Na_2SO_4 was utilized as FS. The *A*, *B* and *R* values were calculated using equations used in our previous study [32].

The structural parameters (*S*, µm) of COF-SPEK membrane were calculated using the following equation (Eq. 4) as also described elsewhere [47].

$$S = \frac{\mathrm{D}}{J_W} \ln \frac{A\pi_d + B}{A\pi_f + B + J_v} \tag{4}$$

Where J_W, *A* and *B* values are obtained from RO test, and π_f (bar) and π_d are the osmotic pressures of FS and DS, respectively. The *D* (m^2 h^{-1}) value indicates the diffusion coefficient of Na_2SO_4.

3 Results and discussion

3.1 Membrane characterization

Figure 2 presents the FTIR spectra of the four SPEK membranes with several COF loadings. The peak at 1650 cm^{-1} occurred from the phenyl ketone group's carbonyl stretching (–Ar–C(=O)–Ar–) [48]. The bands at 1080 cm^{-1} and 1030 cm^{-1} are ascribed to the sulfonic acid group's (O=S=O) symmetric and asymmetric stretching in the SPEK membranes. Additionally, all the COF-incorporated SPEK membranes (COF-10, COF-20 and COF-30) exhibited peaks at 1535 cm^{-1} and 1460 cm^{-1} that are distinctive of the SNW-1 COF's triazine group [49].

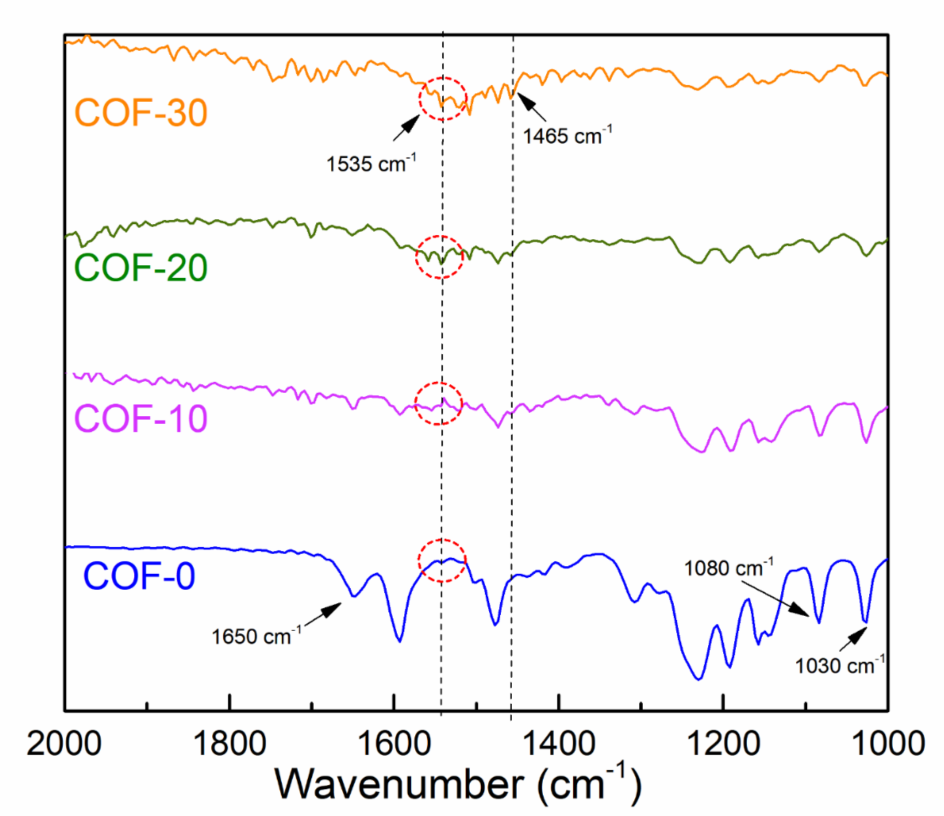

Figure 2. FTIR spectra showing the distinctive peaks of SPEK membranes incorporated with COF nanoparticles at various loadings.

The SEM images in Figure 3 demonstrate the top surface morphologies of pristine and COF-incorporated SPEK membranes prepared in this study. The pristine SPEK membrane (COF-0) is comprised of a flat and smooth top surface, whereas, the COF-incorporated SPEK membranes (COF-10, COF-20 and COF-30) demonstrated rough surfaces with spherical lumps, signifying the presence of COF nanomaterials in the SPEK matrix. The membrane surface became rougher with an increase in COF loading due to their higher proportion relative to the polymer.

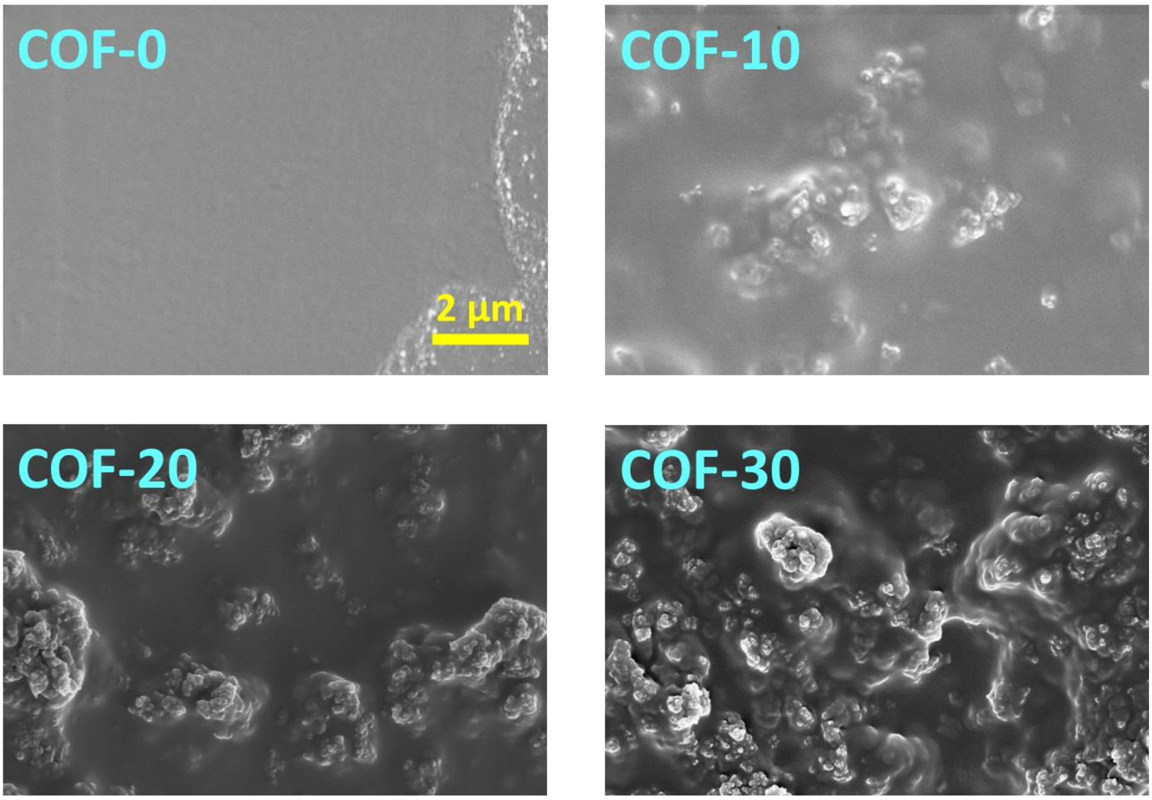

Figure 3. Top surface morphologies of COF-free (COF-0) and COF-incorporated (COF-10, COF-20 and COF-30) SPEK membranes.

Figure 4 presents the cross-section SEM images of the pristine and COF-incorporated SPEK membranes. The virgin COF-0 membrane exhibited a dense and non-porous cross-section morphology with an average thickness of around 600 nm. The presence of COF nanoparticles in the SPEK matrix is clearly visible in the SEM images of COF-20 and COF-30. On the other hand, the cross-section SEM image of the COF-30 membrane showed considerably aggregated COF particles inside the membrane. The thickness of nanocomposite membranes varied from 580 to 610 nm (Table 1) and the non-uniformity in the membrane thickness could be attributed to the different COF loadings.

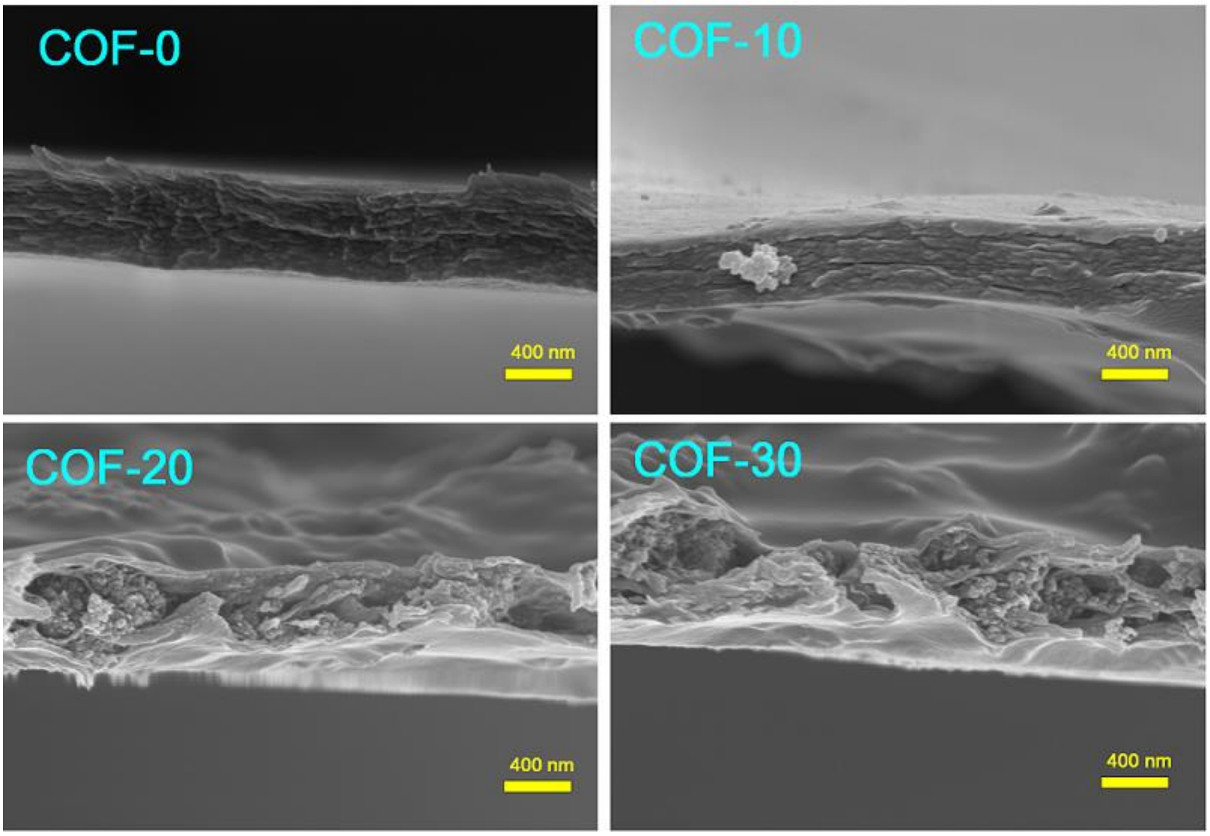

Figure 4. Cross-section images of COF-free (COF-0) and COF-incorporated (COF-10, COF-20 and COF-30) SPEK membranes.

The membrane surface roughness was further characterized by AFM analysis. The AFM images of the SPEK membranes and their mean surface roughness (R_a) are shown in Figure 5. The R_a values of both the top surfaces (Figure 5a) and bottom surfaces (Figure 5b) increased with an increase in COF nanoparticles loading. The pristine SPEK membrane (COF-0) exhibited the smoothest top and bottom surfaces with R_a values of 1.14 nm and 1.03 nm, respectively, whereas COF-30 membrane demonstrated the roughest top and bottom surfaces with R_a values of 133.67 nm and 4.47 nm, respectively, because of the agglomeration of the COF nanoparticles. The roughness of the membrane top surfaces was found to be greater than that of the bottom surfaces due to the COF nanoparticles being primarily located on the top surfaces of the membranes post-fabrication. The increase in membrane surface roughness increases the surface area available for water transport, which could enhance the water flux across the membrane [37, 50].

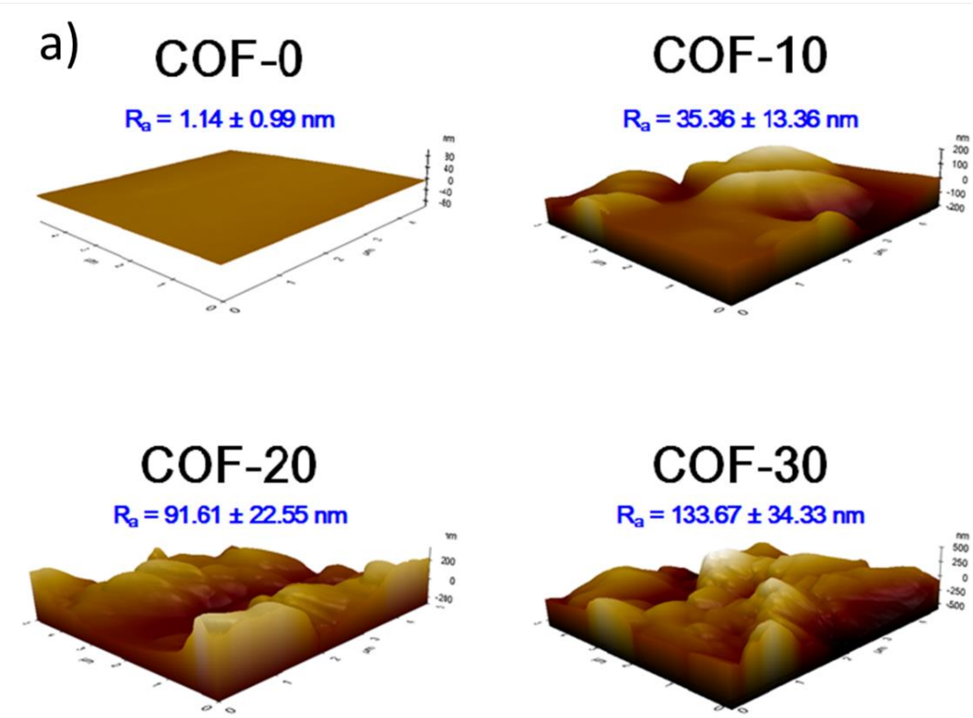

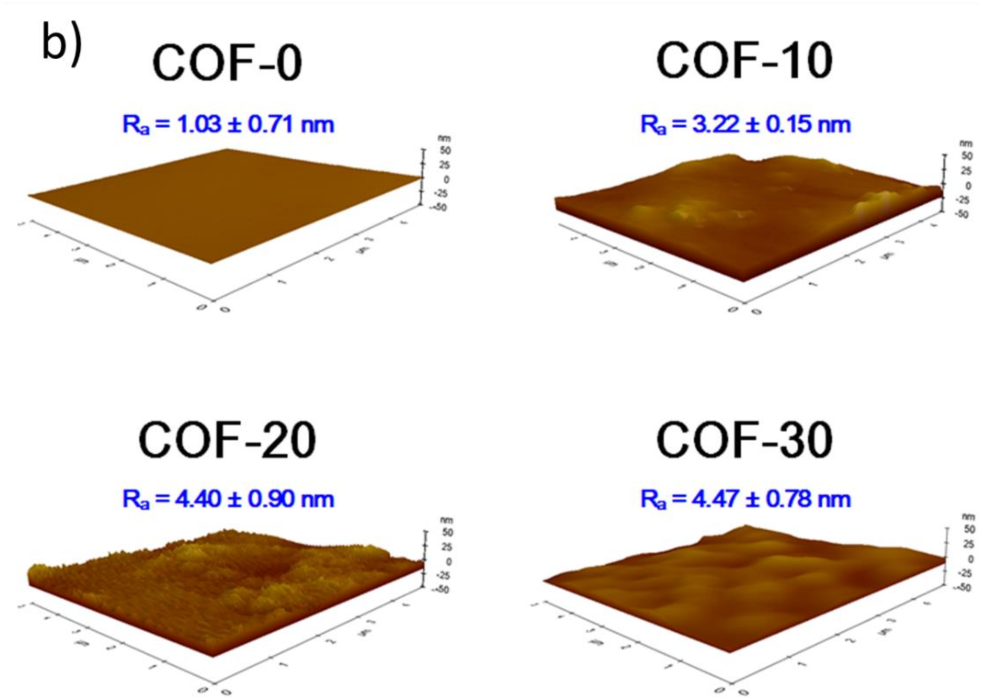

Figure 5. a) Top and b) bottom surface morphologies of COF-free (COF-0) and COF-incorporated (COF-10, COF-20 and COF-30) SPEK membranes.

The hydrophilicity of membrane surface is an important property for improving the water flux. The membrane wettability was assessed from the water contact angles on the membrane surfaces. The incorporation of SNW-1 COF nanoparticles into the SPEK membrane reduced the overall contact angles of both top and bottom surfaces because of the presence of hydrophilic amine functional groups in the SNW-1 COF nanoparticles. In the case of top surface, the contact angle decreased from 92º to around 80º (Figure 6a) with increase of SNW-1 loading up to 30%. The addition of 10% SNW-1 in the SPEK membrane resulted in a lower contact angle value than the COF-free membrane (COF-0). However, the addition of COF loading greater than 10% caused a marginal increase in contact angle values on the membrane top surface despite an increase in the amount of hydrophilic COF nanoparticles in the SPEK matrix. This observation could be attributed to the significant increase in the top surface roughness of the COF-20 and COF-30 membranes (Figure 5a) as observed in other studies [32, 51]. However, the water contact angles on the membranes' bottom surfaces showed a decreasing trend as the COF loading was increased, while the surface roughness remained similar (Figure 5b). Overall, SNW-1 COF nanoparticles increased the hydrophilicity of the SPEK nanocomposite membrane, which will enhance the water permeability of the SPEK membranes. Moreover, the water contact angles on the top layers were lower than those of the bottom layers of the nanocomposite SPEK membranes as the COF nanoparticles may be mainly located on the top surfaces of the membranes as evident from the AFM images (Figure 5).

The mechanical properties of the SPEK-COF membranes at different SNW-1 nanoparticles loading are shown in Figure 6b. The COF-SPEK membranes demonstrated a stable tensile strength and a gradually decreasing elongation at break between SNW-1 loadings of 0-20 wt%. These trends suggest that SNW-1 loading up to 20 wt% has no substantial influence on the mechanical property of the SPEK membranes; thus, indicating a good dispersion of SNW-1 nanoparticles into the SPEK polymer matrix. However, increasing the SNW-1 loading beyond 20 wt% caused a significant decrease in both the tensile strength and elongation at break of the COF-SPEK membrane. The SNW-1 nanoparticles at 30 wt% loading (COF-30) aggregated in the SPEK matrix resulting in the formation of defects, which eventually formed a mechanically weaker membrane [32].

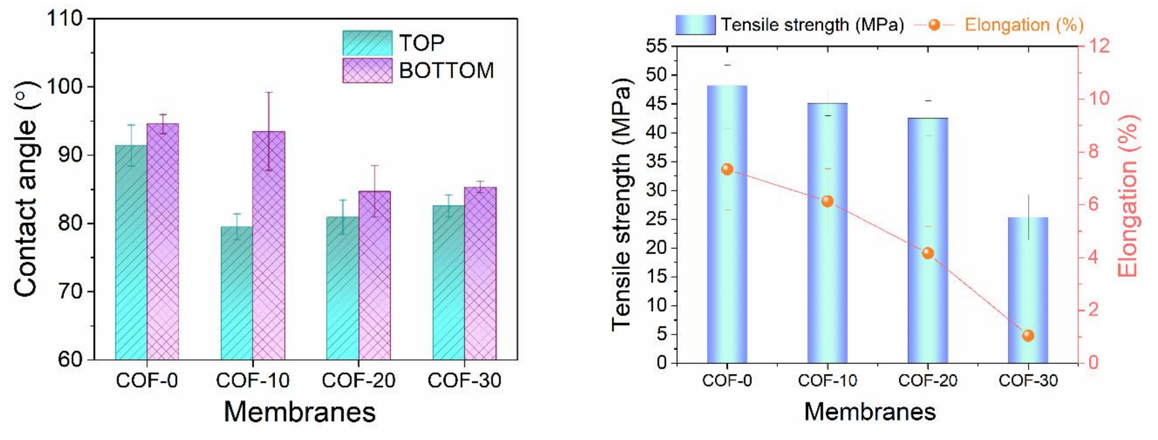

(a) (b)

Figure 6. (a) Contact angle of the top and bottom layers and (b) mechanical properties of the membrane samples.

3.2 Membrane performance in FO process

The FO performances of the pristine and nanocomposite SPEK membranes were evaluated by determining their water flux (J_W), reverse solute flux (J_S) and SRSF (J_S/J_W) as presented in Figure 7. The tests were conducted with 1 M Na_2SO_4 and DI water as DS and FS, respectively. For comparison, the commercial TFC FO membrane (Toray Industry Korea Inc.) was also tested. The water flux of the COF-SPEK membranes increased more than two folds from 12.31 to 28.5 L m^{-2} h^{-1} on increasing the COF loading from 0 to 20 wt% due to formation of more water-selective channels by SNW-1 nanoparticles (Figure 7a) [40]. The pore size of SNW-1 particles is around 5.5 Å that is bigger than the water molecule size, thus allowing water molecules to easily pass through the pores [40]. Moreover, SNW-1 nanoparticles' amine functional groups can adsorb water molecules by forming hydrogen bonds with –OH groups of water molecules [38]. The higher membrane water flux of COF-20 could also be ascribed to its higher surface roughness (Figure 5) and hydrophilicity than that of the COF-10 membrane (Figure 6) as discussed previously.

However, the water flux of the COF-SPEK membrane dropped on increasing the COF loading beyond 20 wt% as evident from the COF-30 membrane's low water flux. It is expected that the COF nanoparticles considerably aggregated in the SPEK membrane at a loading of 30%, which could have created some defects that increased SRSF, thus reducing the osmotic pressure difference between DS and FS. As a consequence, the water flux decreased due to increase in the ICP [33].

The SRSF (J_S/J_W) of the COF-0 membrane was observed to be highest at around 0.17 g L^{-1}. The SRSF of COF-SPEK membranes substantially declined from 0.17 to 0.05 g L^{-1} on increasing the COF loading from 0 to 20 wt% (Figure 7b), which is a desirable feature for FO operation. It can be seen in Figure 7b that the COF-20 showed the smallest SRSF value of 0.05 g L^{-1} among the SPEK membranes. However, increasing the COF loading to 30 wt% caused a drastic increase to the SRSF value (0.14 g L^{-1}). Therefore, it can be confirmed from the FO performance results in this study that the optimum loading of SNW-1 COF nanoparticles in SPEK membranes is 20 wt%. Interestingly, the optimum COF-20 membrane revealed better FO performance than the benchmark commercial TFC FO membrane, which showed a SRSF of 0.08 g L^{-1} and water flux of 24.6 L m^{-2} h^{-1}. This could be attributed to the synergic effects of size exclusion by the COF nanochannels and strong electrostatic repulsion by the membrane barrier with negatively charged sulfonate groups ($-SO_3H$) [52].

Meanwhile, The FO performances of the membrane samples were also tested using 1 M NaCl as DS and DI water as FS (Figure S1). As can be observed from the results, all the COF-SPEK membranes (COF loadings 0-30 %) demonstrated a similar trend in FO performance with both Na_2SO_4 and NaCl as DS but FO performance with the former was superior. The COF-SPEK membranes exhibited enhanced ion selectivity with 1 M Na_2SO_4 (7.6 Å) DS due to its larger hydrated anion size and a higher size-exclusion rate compared to that of NaCl (5.64 Å). Consequently, the COF-incorporated membrane revealed a SRSF of 0.04 – 0.16 g.L^{-1} with Na_2SO_4 DS and 3.5 – 6 g.L^{-1} with NaCl DS [53]. Moreover, the presence of negatively charged sulfonate groups ($-SO_3H$) in the SPEK polymer might further enhance the selectivity of SO_4^{2-} divalent ion [52]. These results confirm that using Na_2SO_4 as DS for COF-SPEK membranes is more suitable than NaCl.

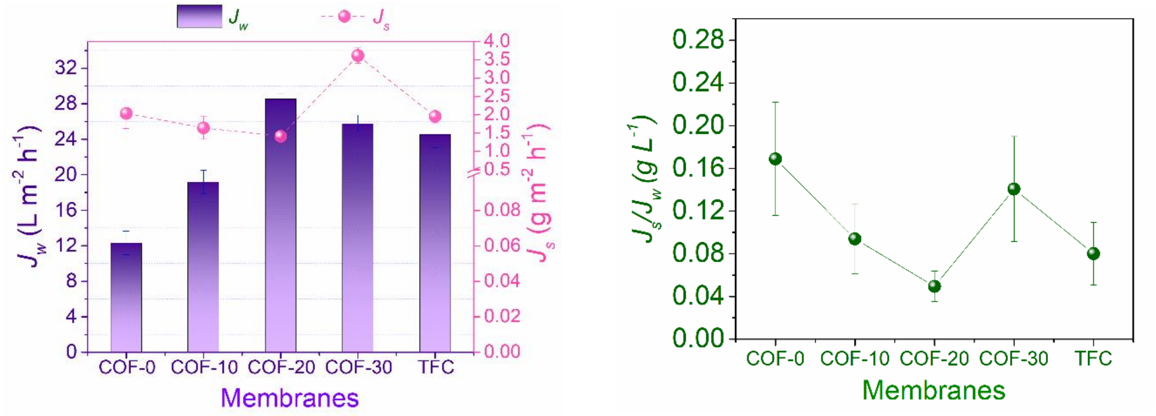

(a) (b)

Figure 7. FO test results of the prepared SPEK membranes and commercial TFC FO membrane from Toray determined with 1 M Na_2SO_4 DS and DI water FS: (a) water flux (J_W) and reverse solute flux (J_S), (b) SRSF (J_S / J_W).

The relative reverse solute flux, water flux and SRSF profiles of the COF-SPEK membranes under various Na_2SO_4 concentrations (0.25 to 1 M) as DS are indicated in Figure 8. As anticipated, the water flux linearly increased with rising DS concentration for all membranes because of the increasing osmotic driving force (Figure 8a) [54]. The linear correlation between the water flux and DS concentration further demonstrates the minimal occurrence of ICP effects due to the symmetric nature and ultra-thin thickness (~700 nm) of the membrane [55, 56]. The reverse solute flux across all the membranes also showed a linear growth with the increase in DS concentration (Figure 8b). The reverse solute flux increased at higher DS concentration because of a higher solute concentration difference across the membrane, which caused a higher draw solute diffusion towards the FS. The SRSF values of the membrane samples, on the other hand, were stable with the variation of DS concentration (Figure 8c), which indicates that the membranes' ion selectivity remained the same regardless of the difference in osmotic pressure. The COF-20 membrane was the optimal COF-SPEK membrane as it revealed the most favourable performance with the lowest SRSF and highest water flux of

0.05 g L^{-1} and 28.54 L m^{-2} h^{-1}, respectively when experimented with 1 M Na_2SO_4 DS and DI water FS.

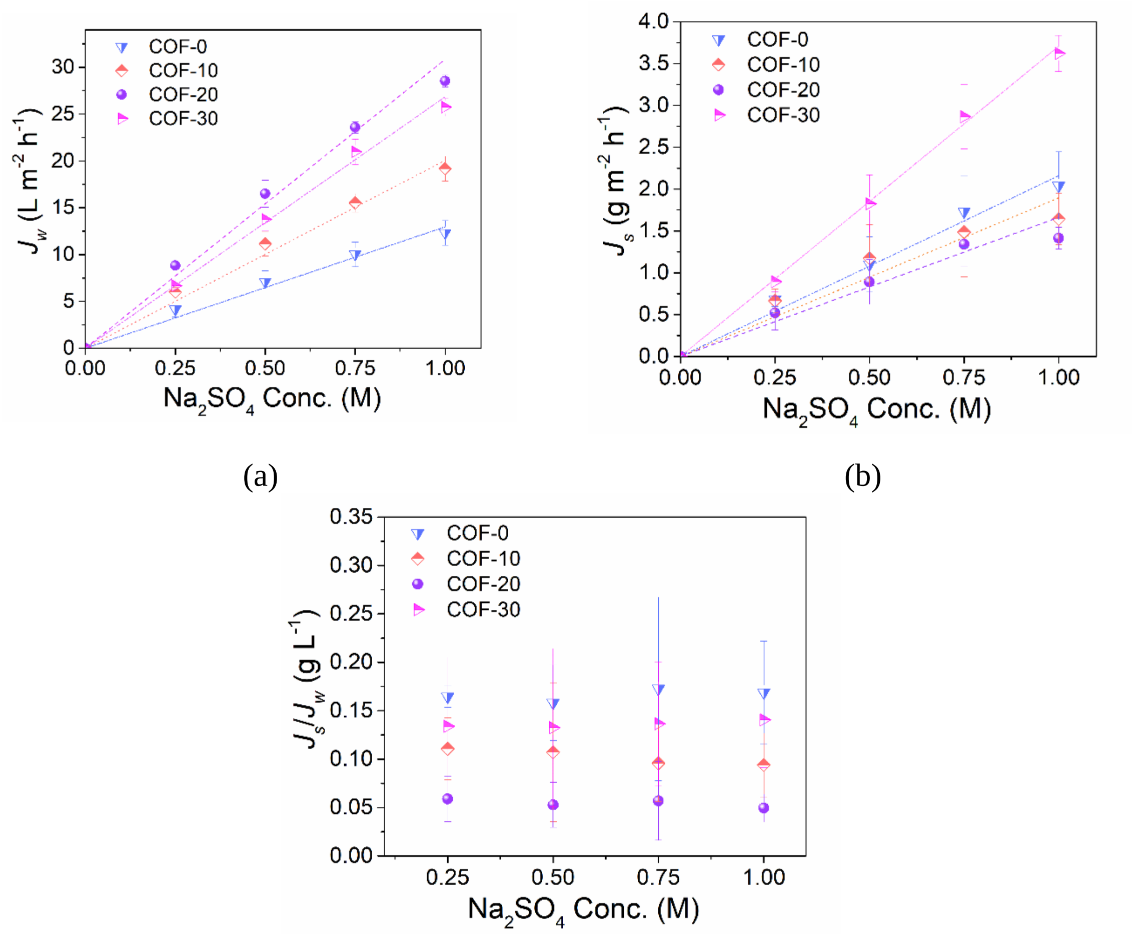

(a) (b)

(c)

Figure 8. FO performance profiles of the prepared SPEK membranes determined by varying the Na_2SO_4 DS concentration from 0.25 to 1 M and using DI water as FS: (a) water flux (J_W), (b) reverse solute flux (J_S) and (c) SRSF (J_S/J_W).

The stability of self-standing COF-20 membrane was further evaluated from its FO performance during long-term membrane operation (12 h) under a cross-flow velocity of 8.3 cm s^{-1} with 1M Na_2SO_4 DS and DI water FS as shown in Figure 9**.** The initial water flux was about 28.0 L m^{-2} h^{-1} employing Na_2SO_4 as DS, which gradually decreased to around 25.0 L m^{-2} h^{-1} (~ 11% flux reduction) following 12 h of operation. The reduction in water flux resulted from the constant dilution of DS, which decreased the osmotic pressure from 46.33 bar (1M Na_2SO_4) to 41.21 bar (0.8809 M Na_2SO_4) as the experiment was operated in batch mode for

12 h, which diluted the Na_2SO_4 DS by about 11%. The decline in FO flux and osmotic pressure as a function of operation time is shown in Figure S2. As evident, the reduction in water flux and osmotic pressure with time are well-matched. However, the SRSF remained at below 0.06 g L^{-1} throughout the FO operation with Na_2SO_4 DS, confirming the good mechanical stability of self-standing FO (COF-20) membrane.

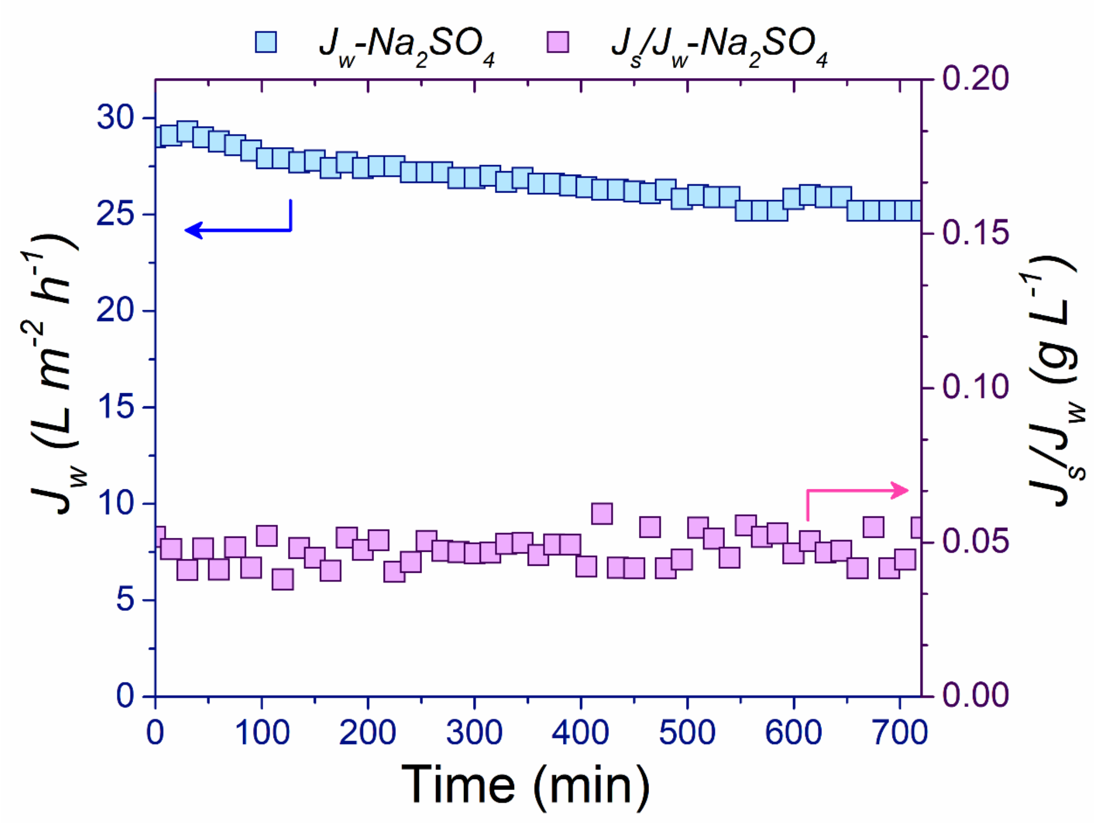

Figure 9. Long-term FO performance of the optimum SPEK nanocomposite membrane (COF-20) under 12 h of operation (DS:1 M Na_2SO_4; FS: DI water).

Figure 10 presents the expected mechanism of water and ion transport across the SPEK-COF membrane. Based on FO performances of the COF-SPEK membranes using different DSs, it is evident that the SNW-1 COF nanoparticles with a pore size of 5 Å can effectively separate large sulfate ions (SO_4^{2-}), which are 7.6 Å in size when incorporated in the SPEK membrane.

Additionally, the existence of 40% sulfonated functional group in the SPEK matrix could mitigate the transportation of sulfate ions across the membrane due to the charge repulsion between SO_4^{2-} and negatively charged sulfonate groups (SO_3H).

The thickness and intrinsic transport properties of the pristine and COF-SPEK membranes are presented in Table 1. The thickness of COF-SPEK membranes was nearly the same in the range of 580-610 nm as the membrane casting height was fixed at 80 µm for all prepared membranes. However, the increased surface roughness (Figure 5a) resulting from the aggregation of COF nanoparticles slightly influenced the uniformity of membrane thickness. The integration of COF nanoparticles into the SPEK membranes heightened the *A* values of all the membranes because of the increased membrane hydrophilicity occurring from the hydrophilic amine groups in the SNW-1 nanoparticles. Also, the porous SNW-1 nanoparticles might have created passages for the water molecules' transport through the membrane. The COF-20 membrane demonstrated an *A* value of $0.68\ \mathrm{L\ m^{-2}\ h^{-1}\ bar^{-1}}$, and a *B* value of the $0.38\ \mathrm{L\ m^{-2}\ h^{-1}}$. The rejection of Na_2SO_4 (R) by the COF-20 membrane was the highest at 96.3% compared to the SPEK membranes investigated in this study. Moreover, the COF-20 membrane demonstrated the smallest *S* value of 5.3 µm compared to other membranes, thus suggesting the positive effect of adding 20 wt% SNW-1 that improved the membrane permeability, porosity and formed the shortest diffusive path length for water molecules' diffusion through the COF-SPEK membrane with minimal defect formation by the COF aggregations.

Conversely, the COF-30 membrane demonstrated the highest *A* ($0.86\ \mathrm{L\ m^{-2}\ h^{-1}\ bar^{-1}}$) and *B* ($0.64\ \mathrm{L\ m^{-2}\ h^{-1}}$) values with lowest R of 94% than the other membranes because of the formation of some membrane defects from aggregated SNW-1 nanoparticles as evident from the cross-sectional SEM image (Figure 4) and considerably high surface roughness (Figure 5a). Therefore, it can be deduced that COF-20 is the optimum SPEK membrane fabricated in this study with the most suitable morphology for water transport.

Table 1. Thickness and intrinsic transport properties of the COF-SPEK membranes at various SNW-1 loading.

Membrane	Thickness (nm)	A-value (L m^{-2} h^{-1} bar^{-1})	B-value (L m^{-2} h^{-1})	R (%)	S value (μm)
COF-0	600	0.34	0.44	95.8	56.5
COF-10	580	0.43	0.41	96.0	7.1
COF-20	590	0.68	0.38	96.3	5.3
COF-30	610	0.86	0.64	94.0	53.7

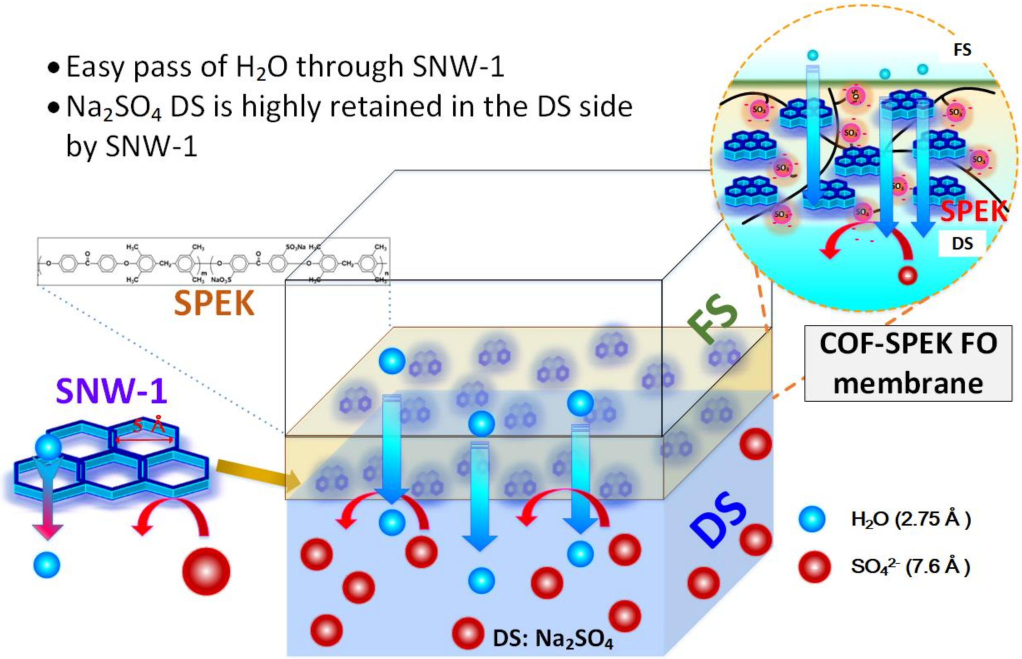

Figure 10. Expected mechanism of the water and ion transport across COF-incorporated SPEK nanocomposite membrane.

4 Conclusions

A novel ultrathin COF-based nanocomposite SPEK (COF-SPEK) FO membrane was successfully developed by integrating various quantities of SNW-1 nanoparticles, varying from 0 to 30 wt%, into the SPEK matrix. Results demonstrated that addition of SNW-1 nanoparticles augmented the surface roughness and hydrophilicity of the SPEK membranes. The SNW-1 nanoparticles' amine functional groups increased the SPEK membranes' hydrophilicity. The best SPEK membrane integrated with 20 wt% SNW-1 COF nanoparticles (COF-20) demonstrated a high water flux of 28.5 L m^{-2} h^{-1} and an extremely low SRSF of 0.05 g L^{-1} using 1 M Na_2SO_4 DS and DI water FS during the FO test. The performance of nanocomposite SPEK membrane worsened on increasing the COF loading beyond 20 wt% due to aggregation of COF nanoparticles in the SPEK matrix resulting in the formation of defects. Consequently, the COF-30 membrane demonstrated the poorest FO performance with a significantly high SRSF of 0.15 g L^{-1}. These outcomes suggest that SNW-1 could be used as nanofillers for bettering the SPEK membranes' FO performance.

CRediT authorship contribution statement

Myoung Jun Park: Conceptualization, Formal analysis, Data curation, Investigation, Validation, Writing – original draft, review & editing. **Nawshad Akther:** Investigation, Methodology, Writing - original draft, Validation, review and editing. **Sherub Phuntsho:** Writing - review & editing. **Gayathri Naidu:** Writing - review & editing. **Amir Razmjou:** Writing - review & editing. **Hokyong Shon:** Conceptualization, Supervision, Writing - review & editing, Resources, Funding acquisition, Project administration.

Declaration of competing interest

The authors declare that they have no known personal relationships or competing financial interests that could have appeared to influence the work reported in this paper.

Acknowledgment

This research was supported by the ARC Industrial Transformation Research Hub (IH170100009) and an internal grant from Mitsui Chemicals, Inc. Japan.

References

[1] A. Giwa, N. Akther, V. Dufour, S.W. Hasan, A critical review on recent polymeric and nano-enhanced membranes for reverse osmosis, RSC Advances, 6 (2016) 8134-8163.

[2] N. Akther, A. Sodiq, A. Giwa, S. Daer, H.A. Arafat, S.W. Hasan, Recent advancements in forward osmosis desalination: A review, Chemical Engineering Journal, 281 (2015) 502-522.

[3] T.Y. Cath, A.E. Childress, M. Elimelech, Forward osmosis: Principles, applications, and recent developments, Journal of Membrane Science, 281 (2006) 70-87.

[4] V.H. Tran, S. Lim, D.S. Han, N. Pathak, N. Akther, S. Phuntsho, H. Park, H.K. Shon, Efficient fouling control using outer-selective hollow fiber thin-film composite membranes for osmotic membrane bioreactor applications, Bioresource Technology, 282 (2019) 9-17.

[5] N. Akther, Y. Lin, S. Wang, S. Phuntsho, Q. Fu, N. Ghaffour, H. Matsuyama, H.K. Shon, In situ ultrathin silica layer formation on polyamide thin-film composite membrane surface for enhanced forward osmosis performances, Journal of Membrane Science, (2020) 118876.

[6] H.G. Zeweldi, A.P. Bendoy, M.J. Park, H.K. Shon, H.-S. Kim, E.M. Johnson, H. Kim, S.-P. Lee, W.-J. Chung, G.M. Nisola, Tetrabutylammonium 2,4,6-trimethylbenzenesulfonate as an effective and regenerable thermo-responsive ionic liquid drawing agent in forward osmosis for seawater desalination, Desalination, 495 (2020) 114635.

[7] S. Daer, N. Akther, Q. Wei, H.K. Shon, S.W. Hasan, Influence of silica nanoparticles on the desalination performance of forward osmosis polybenzimidazole membranes, Desalination, 491 (2020) 114441.

[8] A. Achilli, A.E. Childress, Pressure retarded osmosis: From the vision of Sidney Loeb to the first prototype installation — Review, Desalination, 261 (2010) 205-211.

[9] B.E. Logan, M. Elimelech, Membrane-based processes for sustainable power generation using water, Nature, 488 (2012) 313.

[10] J. Zhang, Q. She, V.W.C. Chang, C.Y. Tang, R.D. Webster, Mining nutrients (N, K, P) from urban source-separated urine by forward osmosis dewatering, Environmental Science & Technology, 48 (2014) 3386-3394.

[11] D. Attarde, M. Jain, P.K. Singh, S.K. Gupta, Energy-efficient seawater desalination and wastewater treatment using osmotically driven membrane processes, Desalination, 413 (2017) 86-100.

[12] N. Akther, V. Sanahuja-Embuena, R. Górecki, S. Phuntsho, C. Helix-Nielsen, H.K. Shon, Employing the synergistic effect between aquaporin nanostructures and graphene oxide for enhanced separation performance of thin-film nanocomposite forward osmosis membranes, Desalination, 498 (2021) 114795.

[13] J.R. McCutcheon, M. Elimelech, Influence of concentrative and dilutive internal concentration polarization on flux behavior in forward osmosis, Journal of Membrane Science, 284 (2006) 237-247.

[14] S. Phuntsho, J.E. Kim, V.H. Tran, S. Tahara, N. Uehara, N. Maruko, H. Matsuno, S. Lim, H.K. Shon, Free-standing, thin-film, symmetric membranes: Next-generation membranes for engineered osmosis, Journal of Membrane Science, 607 (2020) 118145.

[15] N. Akther, S.M. Ali, S. Phuntsho, H. Shon, Surface modification of thin-film composite forward osmosis membranes with polyvinyl alcohol–graphene oxide composite hydrogels for antifouling properties, Desalination, 491 (2020) 114591.

[16] G.T. Gray, J.R. McCutcheon, M. Elimelech, Internal concentration polarization in forward osmosis: role of membrane orientation, Desalination, 197 (2006) 1-8.

[17] N. Akther, S. Daer, Q. Wei, I. Janajreh, S.W. Hasan, Synthesis of polybenzimidazole (PBI) forward osmosis (FO) membrane and computational fluid dynamics (CFD) modeling of concentration gradient across membrane surface, Desalination, 452 (2019) 17-28.

[18] Q. Liu, J. Li, Z. Zhou, J. Xie, J.Y. Lee, Hydrophilic mineral coating of membrane substrate for reducing internal concentration polarization (ICP) in forward osmosis, Scientific Reports, 6 (2016).

[19] R.R. Darabi, M. Peyravi, M. Jahanshahi, A.A. Qhoreyshi Amiri, Decreasing ICP of forward osmosis (TFN-FO) membrane through modifying PES-Fe3O4 nanocomposite substrate, Korean Journal of Chemical Engineering, 34 (2017) 2311-2324.

[20] W. Xu, Q. Chen, Q. Ge, Recent advances in forward osmosis (FO) membrane: Chemical modifications on membranes for FO processes, Desalination, 419 (2017) 101-116.

[21] W.A. Suwaileh, D.J. Johnson, S. Sarp, N. Hilal, Advances in forward osmosis membranes: Altering the sub-layer structure via recent fabrication and chemical modification approaches, Desalination, 436 (2018) 176-201.

[22] Y.-N. Wang, K. Goh, X. Li, L. Setiawan, R. Wang, Membranes and processes for forward osmosis-based desalination: Recent advances and future prospects, Desalination, 434 (2018) 81-99.

[23] M.J. Park, R.R. Gonzales, A. Abdel-Wahab, S. Phuntsho, H.K. Shon, Hydrophilic polyvinyl alcohol coating on hydrophobic electrospun nanofiber membrane for high performance thin film composite forward osmosis membrane, Desalination, 426 (2018) 50-59.

[24] N.-N. Bui, M.L. Lind, E.M.V. Hoek, J.R. McCutcheon, Electrospun nanofiber supported thin film composite membranes for engineered osmosis, J. Membr. Sci., 385-386 (2011) 10-19.

[25] M. Obaid, Z.K. Ghouri, O.A. Fadali, K.A. Khalil, A.A. Almajid, N.A.M. Barakat, Amorphous SiO2 NP-Incorporated Poly(vinylidene fluoride) Electrospun Nanofiber Membrane for High Flux Forward Osmosis Desalination, ACS Appl. Mater. Interfaces, 8 (2016) 4561-4574.

[26] N. Akther, S. Phuntsho, Y. Chen, N. Ghaffour, H.K. Shon, Recent advances in nanomaterial-modified polyamide thin-film composite membranes for forward osmosis processes, Journal of Membrane Science, 584 (2019) 20-45.

[27] M. Fathizadeh, A. Aroujalian, A. Raisi, Effect of added NaX nano-zeolite into polyamide as a top thin layer of membrane on water flux and salt rejection in a reverse osmosis process, Journal of Membrane Science, 375 (2011) 88-95.

[28] N. Ma, J. Wei, R. Liao, C.Y. Tang, Zeolite-polyamide thin film nanocomposite membranes: Towards enhanced performance for forward osmosis, Journal of Membrane Science, 405-406 (2012) 149-157.

[29] X. Liu, H.Y. Ng, Fabrication of layered silica–polysulfone mixed matrix substrate membrane for enhancing performance of thin-film composite forward osmosis membrane, Journal of Membrane Science, 481 (2015) 148-163.

[30] J. Zhang, Z. Xu, W. Mai, C. Min, B. Zhou, M. Shan, Y. Li, C. Yang, Z. Wang, X. Qian, Improved hydrophilicity, permeability, antifouling and mechanical performance of PVDF composite ultrafiltration membranes tailored by oxidized low-dimensional carbon nanomaterials, Journal of Materials Chemistry A, 1 (2013) 3101-3111.

[31] L. Wang, X. Song, T. Wang, S. Wang, Z. Wang, C. Gao, Fabrication and characterization of polyethersulfone/carbon nanotubes (PES/CNTs) based mixed matrix membranes (MMMs) for nanofiltration application, Applied Surface Science, 330 (2015) 118-125.

[32] M.J. Park, S. Phuntsho, T. He, G.M. Nisola, L.D. Tijing, X.-M. Li, G. Chen, W.-J. Chung, H.K. Shon, Graphene oxide incorporated polysulfone substrate for the fabrication of flat-sheet thin-film composite forward osmosis membranes, Journal of Membrane Science, 493 (2015) 496-507.

[33] N. Akther, Y. Kawabata, S. Lim, T. Yoshioka, S. Phuntsho, H. Matsuyama, H.K. Shon, Effect of graphene oxide quantum dots on the interfacial polymerization of a thin-film nanocomposite forward osmosis membrane: An experimental and molecular dynamics study, Journal of Membrane Science, 630 (2021) 119309.

[34] S. Lim, K.H. Park, V.H. Tran, N. Akther, S. Phuntsho, J.Y. Choi, H.K. Shon, Size-controlled graphene oxide for highly permeable and fouling-resistant outer-selective hollow fiber thin-film composite membranes for forward osmosis, Journal of Membrane Science, 609 (2020) 118171.

[35] N. Akther, Z. Yuan, Y. Chen, S. Lim, S. Phuntsho, N. Ghaffour, H. Matsuyama, H. Shon, Influence of graphene oxide lateral size on the properties and performances of forward osmosis membrane, Desalination, 484 (2020) 114421.

[36] C. Zhang, M. Huang, L. Meng, B. Li, T. Cai, Electrospun polysulfone (PSf)/titanium dioxide (TiO2) nanocomposite fibers as substrates to prepare thin film forward osmosis membranes, Journal of Chemical Technology & Biotechnology, 92 (2017) 2090-2097.

[37] D. Emadzadeh, W.J. Lau, T. Matsuura, M. Rahbari-Sisakht, A.F. Ismail, A novel thin film composite forward osmosis membrane prepared from PSf–TiO2 nanocomposite substrate for water desalination, Chemical Engineering Journal, 237 (2014) 70-80.

[38] S. Lim, N. Akther, V.H. Tran, T.-H. Bae, S. Phuntsho, A. Merenda, L.F. Dumée, H.K. Shon, Covalent organic framework incorporated outer-selective hollow fiber thin-film

nanocomposite membranes for osmotically driven desalination, Desalination, 485 (2020) 114461.

[39] C. Li, S. Li, L. Tian, J. Zhang, B. Su, M.Z. Hu, Covalent organic frameworks (COFs)-incorporated thin film nanocomposite (TFN) membranes for high-flux organic solvent nanofiltration (OSN), Journal of Membrane Science, 572 (2019) 520-531.

[40] N. Akther, S. Lim, V.H. Tran, S. Phuntsho, Y. Yang, T.-H. Bae, N. Ghaffour, H.K. Shon, The effect of Schiff base network on the separation performance of thin film nanocomposite forward osmosis membranes, Separation and Purification Technology, 217 (2019) 284-293.

[41] H.-G. Yuan, Y.-Y. Liu, T.-Y. Liu, X.-L. Wang, Self-standing nanofilms of polysulfone doped with sulfonated polysulfone via solvent evaporation for forward osmosis, Journal of Membrane Science, 523 (2017) 567-575.

[42] M. Li, V. Karanikola, X. Zhang, L. Wang, M. Elimelech, A Self-Standing, Support-Free Membrane for Forward Osmosis with No Internal Concentration Polarization, Environmental Science & Technology Letters, 5 (2018) 266-271.

[43] H. Liu, H. Wang, X. Zhang, Facile Fabrication of Freestanding Ultrathin Reduced Graphene Oxide Membranes for Water Purification, Advanced Materials, 27 (2015) 249-254.

[44] R.R. Gonzales, M.J. Park, T.-H. Bae, Y. Yang, A. Abdel-Wahab, S. Phuntsho, H.K. Shon, Melamine-based covalent organic framework-incorporated thin film nanocomposite membrane for enhanced osmotic power generation, Desalination, 459 (2019) 10-19.

[45] C. Wang, Z. Li, J. Chen, Z. Li, Y. Yin, L. Cao, Y. Zhong, H. Wu, Covalent organic framework modified polyamide nanofiltration membrane with enhanced performance for desalination, Journal of Membrane Science, 523 (2017) 273-281.

[46] X. Wu, Z. Tian, S. Wang, D. Peng, L. Yang, Y. Wu, Q. Xin, H. Wu, Z. Jiang, Mixed matrix membranes comprising polymers of intrinsic microporosity and covalent organic framework for gas separation, Journal of Membrane Science, 528 (2017) 273-283.

[47] T.Y. Liu, H.G. Yuan, Y.Y. Liu, D. Ren, Y.C. Su, X. Wang, Metal-Organic Framework Nanocomposite Thin Films with Interfacial Bindings and Self-Standing Robustness for High Water Flux and Enhanced Ion Selectivity, ACS Nano, 12 (2018) 9253-9265.

[48] V.S. Rangasamy, S. Thayumanasundaram, J.W. Seo, J.-P. Locquet, Vibrational spectroscopic study of pure and silica-doped sulfonated poly(ether ether ketone) membranes, Spectrochimica Acta Part A: Molecular and Biomolecular Spectroscopy, 138 (2015) 693-699.

[49] M.G. Schwab, B. Fassbender, H.W. Spiess, A. Thomas, X. Feng, K. Müllen, Catalyst-free preparation of melamine-based microporous polymer networks through Schiff base chemistry, Journal of the American Chemical Society, 131 (2009) 7216-7217.

[50] P. Lu, S. Liang, L. Qiu, Y. Gao, Q. Wang, Thin film nanocomposite forward osmosis membranes based on layered double hydroxide nanoparticles blended substrates, Journal of Membrane Science, 504 (2016) 196-205.

[51] M. Shibuya, M.J. Park, S. Lim, S. Phuntsho, H. Matsuyama, H.K. Shon, Novel CA/PVDF nanofiber supports strategically designed via coaxial electrospinning for high performance thin-film composite forward osmosis membranes for desalination, Desalination, 445 (2018) 63-74.

[52] W. Cheng, J. Ma, X. Zhang, M. Elimelech, Sub-1 μm Free-Standing Symmetric Membrane for Osmotic Separations, Environmental Science & Technology Letters, 6 (2019) 492-498.

[53] A. Achilli, T.Y. Cath, A.E. Childress, Selection of inorganic-based draw solutions for forward osmosis applications, Journal of Membrane Science, 364 (2010) 233-241.

[54] N. Akther, S. Daer, S.W. Hasan, Effect of flow rate, draw solution concentration and temperature on the performance of TFC FO membrane, and the potential use of RO reject brine as a draw solution in FO–RO hybrid systems, Desalination and Water Treatment, 136 (2018) 65-71.

[55] S.-M. Shim, W.-S. Kim, A numerical study on the performance prediction of forward osmosis process, J Mech Sci Technol, 27 (2013) 1179-1189.

[56] S. Phuntsho, S. Sahebi, T. Majeed, F. Lotfi, J.E. Kim, H.K. Shon, Assessing the major factors affecting the performances of forward osmosis and its implications on the desalination process, Chem. Eng. J., 231 (2013) 484-496.